Parallel Stokeslet between two coaxially positioned rigid no-slip disks: A dual integral equation approach

Abdallah Daddi-Moussa-Ider*
Institut für Theoretische Physik II: Weiche Materie,
Heinrich-Heine-Universität Düsseldorf, D–40225 Düsseldorf, Germany
(Dated: July 21, 2021)

The hydrodynamic flow field induced by a point-force singularity (Stokeslet) acting parallel to two coaxially positioned no-slip disks of finite size is studied on the basis of the linearized Navier-Stokes equations. The Stokeslet is assumed to be located on the center axis of the two disks. The solution of the hydrodynamic equations is formulated as a mixed-boundary-value problem which is then reduced into a system of six dual integral equations in the inner and outer domains. We show the existence of asymmetric viscous eddies and generation of recirculation vortices in the fluid domain bounded by the two plates and systematically examine the variation of the height of the stagnation point with respect to the geometrical parameters of the system. Additionally, we employ the derived solution to probe the effect of the coaxially positioned disks on the slow parallel motion of a point-like particle and assess the validity of the often-used superposition approximation. Our results may prove useful in the study of the behavior of colloidal suspensions in confined geometries.

An elaborated version including appendices has been submitted to La Houille Blanche – Revue internationale de l'eau / LHB Hydroscience Journal (in French). Title: "Stokeslet parallèle entre deux disques rigides antidérapants positionnés de manière coaxiale : une approche aux équations intégrales duales".

I. INTRODUCTION

Fluid-mediated hydrodynamic interactions between colloidal particles in a solvent medium under confinements are ubiquitous in nature and find application in various industrial and technological processes [1, 2]. A deep understanding of the effect of confining boundaries on the dynamics and rheology of colloidal suspensions is of paramount importance in the design and development of microfluidic systems. Prime examples include particle/cell manipulation in microfluidic chips [3–6], DNA separation and genotyping analysis in nano-capillary channels [7–9], and probing of complex structures in atomic force microscopy measurements [10–13]. Over the past few decades, there has been a tremendous research effort focused on unveiling the behavior of particulate suspension flow in narrow confinements.

At small length and time scales, flowing fluids are governed by low-Reynolds-number hydrodynamics, as long as viscous forces dominate over inertial forces. In these situations, a full description of the mutual interactions between particles suspended in a viscous medium is provided by the hydrodynamic mobilities [14] that bridge the velocity of the particles to the forces exerted on their surfaces. Analytical expressions of the mobility functions are tabulated for diverse types of geometrical confinements, e.g. in the classic textbook by Happel and Brenner [15]. Heretofore, available analytical results include the solution for the hydrodynamic mobility and Brownian motion of a particle settling near a flat wall [16–25], a planar interface with a partial-slip [26–28], a surfactant-covered interface [29–31], a rough surface [32], an elastic membrane featuring shear and bending deformation modes [33–41] or a surface separating two mutually immiscible liquids [42, 43].

In a seminal work, the low-Reynolds-number motion of a colloidal particle moving in a channel bounded by two infinitely extended plates has been examined by Faxén [44]. In his PhD dissertation, Faxén provided perturbative expressions of the translational mobility for parallel motion when the particle is moving in the mid-plane or quarter-plane between two planar walls [15]. An exact solution for arbitrary motion of a point-like particle moving in a channel has later been obtained by Liron [45] using the image solution technique. Likewise, the arbitrary motion of a truly extended particle between two plates has been investigated using multipole expansion [46, 47] or via a combined analytical-numerical technique [48, 49]. Theoretical predictions have been verified using direct imaging measurements [50], dynamic light scattering [51], as well as video microscopy [52] in combination with optical tweezers [53, 54].

In a recent work [55], the axisymmetric Stokes flow induced by a point-like particle moving normal to two coaxially positioned rigid no-slip disks of finite size has analytically been obtained. There, the hydrodynamic problem for the surrounding viscous flow has been formulated as a mixed-boundary-value problem, which has subsequently been reduced into a system of dual integral equations amenable to numerical integration. In the present contribution, we complement and supplement this earlier work by examining, using an analogous approach, the asymmetric flow field induced by a point particle

* daddi-moussa-ider (at) protonmail (dot) ch

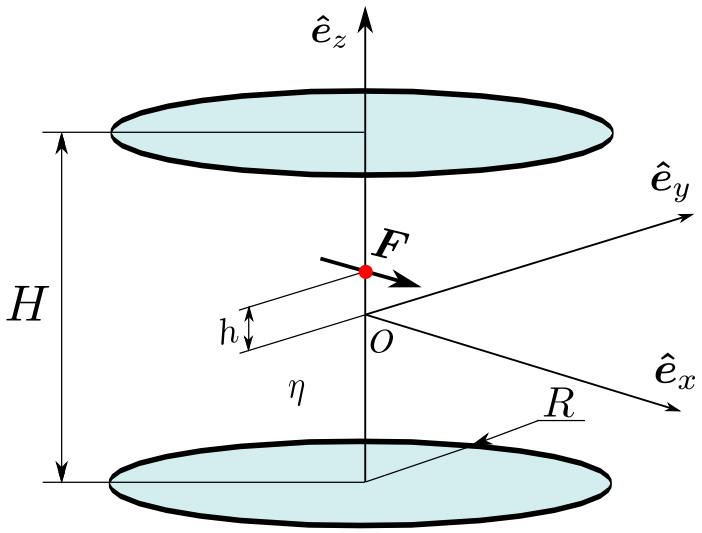

Figure 1. Schematic description showing two coaxially positioned disks of radius R and separation H, and a point force singularity (Stokeslet) acting between them at a height h above the center point O. This Stokeslet is transversely oriented, i.e. acting perpendicular to the axis of symmetry of the setup. The whole setup is embedded in a Newtonian fluid medium of viscosity η.

moving parallel to two finite sized disks. The dual integral equation approach has previously successfully been used to address the flow induced by a Stokeslet near a no-slip disk [56, 57], a finite-sized elastic membrane [58, 59], or the axisymmetric slow viscous flow due to the motion of two coaxially positioned disks of the same size [60].

The remainder of the paper is structured as follows. Firstly, in Sec. II, the physical problem under investigation is described and the governing equations of fluid motion as well as the underlying boundary conditions are introduced. Thereafter, the solution technique using the dual integral approach is outlined. In Sec. III, the results so obtained with regard to the hydrodynamic mobility and flow fields are discussed. Finally, the key outcomes are highlighted and further research directions are provided in Sec. IV.

II. MATHEMATICAL FORMULATION

As introduced above, we examine the low-Reynolds-number fluid flow induced by a Stokeslet singularity acting tangent to the surfaces of two coaxially positioned rigid disks of equal radius R. The disks are located a distance H apart, within the planes $z = -H/2$ and $z = H/2$ of a Cartesian coordinate frame, see Fig. 1. Moreover, the disks are assumed to be infinitesimally thin. More precisely, we consider the situation in which the Stokeslet is located on the axis passing through the centers of the coaxially positioned disks, here described by the z axis. We assume that the flow preserves the volume of the fluid, and we denote by η the viscosity of the surrounding Newtonian fluid filling up the whole space. Subsequently, we scale all lengths by the separation distance H.

A. Governing equations

Under creeping flow conditions, hydrodynamics is then governed by the Stokes equations [15]

$$-\boldsymbol{\nabla} p + \eta \boldsymbol{\nabla}^2 \boldsymbol{v} + \boldsymbol{F}\delta(\boldsymbol{r} - \boldsymbol{r}_0) = \boldsymbol{0}\,, \tag{1a}$$

$$\boldsymbol{\nabla} \cdot \boldsymbol{v} = 0\,, \tag{1b}$$

wherein $\boldsymbol{v}$ and p denote, respectively, the fluid velocity and pressure fields. In addition, $\boldsymbol{F}$ is a concentrated point-force acting on the surrounding fluid at position $\boldsymbol{r}_0 = h\hat{\boldsymbol{e}}_z$ tangent to the two disks, where $h \in (-H/2, H/2)$. The unit vector $\hat{\boldsymbol{e}}_z$ is directed normal to the planes containing the disks, and we choose the origin of our coordinate system as the center point between the two disks. Without loss of generality, we assume that the point-force is oriented along the positive x direction such that $\boldsymbol{F} = F\hat{\boldsymbol{e}}_x$.

We identify by the subscript 1 the flow parameters in the fluid domain beneath the plane containing the lower disk, defined by $z \in (-\infty, -H/2]$, by the subscript 2 the fluid region bounded by the planes containing the two disks such that $z \in [-H/2, H/2]$, and by the subscript 3 the fluid domain above the plane containing the upper disk, defined by $z \in [H/2, \infty)$.

The solution of the fluid dynamics equations (1) in an unbounded fluid medium in the absence of the two disks is expressed in terms of the free-space Green's function [15]. The corresponding velocity components $(v_r^{\mathrm{S}}, v_\phi^{\mathrm{S}}, v_z^{\mathrm{S}})$ are given in the cylindrical coordinate system (r, ϕ, z) by

$$v_r^{\mathrm{S}} = \frac{K}{\rho}\left(1 + \frac{r^2}{\rho^2}\right)\cos\phi\,, \tag{2a}$$

$$v_\phi^{\mathrm{S}} = \frac{K}{\rho}\sin\phi\,, \tag{2b}$$

$$v_z^{\mathrm{S}} = \frac{Kr\,(z-h)}{\rho^3}\cos\phi\,, \tag{2c}$$

where we have used the abbreviation $K = F/(8\pi\eta)$. In addition, the corresponding pressure field is expressed as

$$p^{\mathrm{S}} = \frac{2Kr}{\rho^3}\cos\phi\,, \tag{3}$$

where $\rho = |\boldsymbol{r} - \boldsymbol{r}_0| = \left(r^2 + (z-h)^2\right)^{1/2}$ represents the distance of a point measured from the position of the Stokeslet.

The presence of confining disks can be incorporated in the solution of the flow problem by considering a complementary solution $(\boldsymbol{v}^*, p^*)$ such that its linear superposition with the unbounded flow

$$\boldsymbol{v} = \boldsymbol{v}^{\mathrm{S}} + \boldsymbol{v}^*\,, \qquad p = p^{\mathrm{S}} + p^*\,, \tag{4}$$

satisfies the underlying regularity and boundary conditions. The complementary solution $(\boldsymbol{v}^*, p^*)$ is also sometimes called the image solution [61].

Since the Stokeslet is acting perpendicular to the center axis of the setup, the flow problem becomes asymmetric about the center axis. In this case, the solution of the Stokes flow can conveniently be expressed as [62]

$$\boldsymbol{v}^* = \boldsymbol{\nabla}\Pi + z\boldsymbol{\nabla}\Phi - \Phi\hat{\boldsymbol{e}}_z + \boldsymbol{\nabla}\times(\Omega\,\hat{\boldsymbol{e}}_z)\,, \tag{5a}$$

$$p^* = 2\eta\,\frac{\partial\Phi}{\partial z}\,. \tag{5b}$$

Here Π, Ψ, and Ω are three harmonic functions satisfying Laplace's equation, namely, $\boldsymbol{\nabla}^2\Pi = \boldsymbol{\nabla}^2\Psi = \boldsymbol{\nabla}^2\Omega = 0$, and

$$\Phi = \Psi + \frac{\partial\Pi}{\partial z}\,. \tag{6}$$

The solution of Laplace's equation in the present geometry can be expressed in terms of Fourier-Bessel integrals of the form

$$\Pi_i = K\cos\phi\int_0^\infty \left(A_i^+ e^{\lambda z} + A_i^- e^{-\lambda z}\right) J_1(\lambda r)\,\mathrm{d}\lambda\,, \tag{7a}$$

$$\Psi_i = K\cos\phi\int_0^\infty \left(B_i^+ e^{\lambda z} + B_i^- e^{-\lambda z}\right) J_1(\lambda r)\,\mathrm{d}\lambda\,, \tag{7b}$$

$$\Omega_i = K\sin\phi\int_0^\infty \left(C_i^+ e^{\lambda z} + C_i^- e^{-\lambda z}\right) J_1(\lambda r)\,\mathrm{d}\lambda\,, \tag{7c}$$

where $i \in \{1,2,3\}$ identifies the fluid domain under consideration. Here, λ denotes the wavenumber (with dimension of inverse length), J_1 represents the first-order Bessel function of the first kind [63], and $(A_i^\pm, B_i^\pm, C_i^\pm)$ are unknown wavenumber-dependent functions yet to be determined from the prescribed regularity and boundary conditions outlined in the following.

B. Regularity and boundary conditions

Far away from the singularity position, we require vanishing hydrodynamic fields as $\rho \to \infty$. This leads to $A_1^- = B_1^- = C_1^- = A_3^+ = B_3^+ = C_3^+ = 0$, greatly reducing the number of unknown quantities. Hereinafter, we ease notations by using $A_1^+ \equiv A_1$, $B_1^+ \equiv B_1$, $C_1^+ \equiv C_1$ in domain 1, and $A_3^- \equiv A_3$, $B_3^- \equiv B_3$, $C_3^- \equiv C_3$ in domain 3.

As boundary conditions, we require the continuity of fluid velocities at the domain interfaces. Specifically,

$$\boldsymbol{v}_1 - \boldsymbol{v}_2|_{z=-\frac{1}{2}} = \boldsymbol{v}_2 - \boldsymbol{v}_3|_{z=\frac{1}{2}} = \boldsymbol{0} \qquad (r>0)\,. \tag{8}$$

In addition, we impose, on the one hand, no-slip and no-penetration boundary conditions [26] at the inner domain $(r<R)$ defined by the surface of the disk, yielding

$$\boldsymbol{v}_1|_{z=-\frac{1}{2}} = \boldsymbol{v}_2|_{z=\pm\frac{1}{2}} = \boldsymbol{v}_3|_{z=\frac{1}{2}} = \boldsymbol{0} \qquad (r<R)\,. \tag{9}$$

On the other hand, we require in the outer region $(r > R)$ the natural continuity of the normal stresses at the interfaces between the fluid domains. Specifically,

$$\boldsymbol{T}_2 - \boldsymbol{T}_1|_{z=-\frac{1}{2}} = \boldsymbol{T}_3 - \boldsymbol{T}_2|_{z=\frac{1}{2}} = \boldsymbol{0} \qquad (r>R)\,, \tag{10}$$

where $\boldsymbol{T}_i := \boldsymbol{\sigma}_i\cdot\hat{\boldsymbol{e}}_z$ denotes the hydrodynamic stress vector, having the following form in cylindrical coordinates

$$\begin{aligned}\boldsymbol{T}_i = {}& \eta\left(\frac{\partial v_{ri}}{\partial z} + \frac{\partial v_{zi}}{\partial r}\right)\hat{\boldsymbol{e}}_r + \eta\left(\frac{\partial v_{\phi i}}{\partial z} + \frac{1}{r}\frac{\partial v_{zi}}{\partial\phi}\right)\hat{\boldsymbol{e}}_\phi \\ & + \left(-p_i + 2\eta\,\frac{\partial v_{zi}}{\partial z}\right)\hat{\boldsymbol{e}}_z\,, \quad \text{for } i\in\{1,2,3\}\,.\end{aligned} \tag{11}$$

C. The dual integral formulation

The dual integral equation approach has previously been used successfully to address the flow induced by a Stokeslet near a no-slip disk [56, 57], a finite-sized elastic membrane [58, 59], or to calculate the axisymmetric viscous flow due to the motion of two coaxially positioned disks of the same size [60]. Following a similar approach, the boundary conditions of vanishing velocity components at the surface of the disks in the inner region $(r<R)$ stated by Eq. (9) can be rearranged to give the following six integral equations,

$$\int_0^\infty f_1^-(\lambda)e^{-\frac{\lambda}{2}}J_0(r\lambda)\,\mathrm{d}\lambda = \xi_0^+(r) \qquad (r<R)\,, \tag{12a}$$

$$\int_0^\infty f_3^-(\lambda)e^{-\frac{\lambda}{2}}J_0(r\lambda)\,\mathrm{d}\lambda = \xi_0^-(r) \qquad (r<R)\,, \tag{12b}$$

$$\int_0^\infty q_1^-(\lambda)e^{-\frac{\lambda}{2}}J_1(r\lambda)\,\mathrm{d}\lambda = \xi_1^+(r) \qquad (r<R)\,, \tag{12c}$$

$$\int_0^\infty q_3^+(\lambda)e^{-\frac{\lambda}{2}}J_1(r\lambda)\,\mathrm{d}\lambda = \xi_1^-(r) \qquad (r<R)\,, \tag{12d}$$

$$\int_0^\infty f_1^+(\lambda)e^{-\frac{\lambda}{2}}J_2(r\lambda)\,\mathrm{d}\lambda = \xi_2^+(r) \qquad (r<R)\,, \tag{12e}$$

$$\int_0^\infty f_3^+(\lambda)e^{-\frac{\lambda}{2}}J_2(r\lambda)\,\mathrm{d}\lambda = \xi_2^-(r) \qquad (r<R)\,, \tag{12f}$$

where we have defined, for convenience, the abbreviations

$$f_1^\pm(\lambda) = \tfrac{1}{2}\,\lambda\left((\lambda-2)\,A_1 + B_1 \pm 2C_1\right)\,, \tag{13a}$$

$$f_3^\pm(\lambda) = \tfrac{1}{2}\,\lambda\left((\lambda-2)\,A_3 - B_3 \pm 2C_3\right)\,, \tag{13b}$$

$$q_i^\pm(\lambda) = \tfrac{1}{2}\left(\pm A_i\lambda^2 - (\lambda+2)B_i\right) \tag{13c}$$

and used the recurrence relation of Bessel functions [63]

$$\frac{2k}{\lambda r}\,J_k(\lambda r) = J_{k-1}(\lambda r) + J_{k+1}(\lambda r)\,. \tag{14}$$

The radial functions appearing on the right hand side of Eqs. (12) carry the signature of the free-space velocity field due to the Stokeslet and are explicitly given by

$$\xi_0^\pm(r) = \frac{3r^2 + 2(h\pm\frac{1}{2})^2}{\left(r^2 + (h\pm\frac{1}{2})^2\right)^{3/2}}\,, \tag{15a}$$

$$\xi_1^\pm(r) = \frac{(h\pm\frac{1}{2})r}{\left(r^2 + (h\pm\frac{1}{2})^2\right)^{3/2}}\,, \tag{15b}$$

$$\xi_2^{\pm}(r) = \frac{-r^2}{\left(r^2 + (h \pm \frac{1}{2})^2\right)^{3/2}}. \tag{15c}$$

Subsequently, the boundary conditions related to the continuity of tangential stresses in the outer region ($r > R$) stated by Eq. (10) can likewise be expressed in terms of integral equations as

$$\int_0^\infty g_i(\lambda) J_1(\lambda r)\,\mathrm{d}\lambda = 0 \qquad (r > R)\,, \quad i \in \{1,4\}\,, \tag{16a}$$

$$\int_0^\infty g_i(\lambda) J_0(\lambda r)\,\mathrm{d}\lambda = 0 \qquad (r > R)\,, \quad i \in \{2,5\}\,, \tag{16b}$$

$$\int_0^\infty g_i(\lambda) J_2(\lambda r)\,\mathrm{d}\lambda = 0 \qquad (r > R)\,, \quad i \in \{3,6\}\,, \tag{16c}$$

where g_i's form the vector $\boldsymbol{g} = (g_1, g_2, g_3, g_4, g_5, g_6)^{\mathrm{T}}$ and are unknown wavenumber-dependent quantities, given by

$$\boldsymbol{g} = \boldsymbol{\Lambda}_{13} \cdot \boldsymbol{\mathcal{Z}}_{13} + \boldsymbol{\Lambda}_2 \cdot \boldsymbol{\mathcal{Z}}_2\,. \tag{17}$$

Here,

$$\boldsymbol{\Lambda}_{13} = \begin{pmatrix} \boldsymbol{\Lambda}^+ & \mathbf{0} \\ \mathbf{0} & \boldsymbol{\Lambda}^- \end{pmatrix}, \tag{18}$$

where we have defined the submatrices

$$\boldsymbol{\Lambda}^{\pm} = \begin{pmatrix} -\lambda\sigma^- & \mp\varphi_+^- & 0 \\ \pm\lambda\varphi_-^- & \sigma^- & \mp\sigma^- \\ \pm\lambda\varphi_-^- & \sigma^- & \pm\sigma^- \end{pmatrix}, \tag{19}$$

with $\varphi_+^{\pm} = \lambda(\lambda+2)\,e^{\pm\frac{\lambda}{2}}$, $\varphi_-^{\pm} = \lambda(\lambda-2)\,e^{\pm\frac{\lambda}{2}}$, and $\sigma^{\pm} = \lambda^2 e^{\pm\frac{\lambda}{2}}$. In addition

$$\boldsymbol{\Lambda}_2 = \begin{pmatrix} \boldsymbol{\Lambda}_1^+ & \boldsymbol{\Lambda}_2^+ \\ \boldsymbol{\Lambda}_1^- & \boldsymbol{\Lambda}_2^- \end{pmatrix}, \tag{20}$$

where we have defined

$$\boldsymbol{\Lambda}_1^{\pm} = \begin{pmatrix} \pm\lambda\sigma^{\mp} & \mp\lambda\sigma^{\pm} & \pm\varphi_{\pm}^{\mp} \\ \mp\lambda\varphi_{\mp}^{\mp} & \mp\lambda\varphi_{\pm}^{\pm} & \mp\sigma^{\mp} \\ \mp\lambda\varphi_{\mp}^{\mp} & \mp\lambda\varphi_{\pm}^{\pm} & \mp\sigma^{\mp} \end{pmatrix} \tag{21}$$

and

$$\boldsymbol{\Lambda}_2^{\pm} = \begin{pmatrix} \pm\varphi_{\mp}^{\pm} & 0 & 0 \\ \pm\sigma^{\pm} & \sigma^{\mp} & -\sigma^{\pm} \\ \pm\sigma^{\pm} & -\sigma^{\mp} & \sigma^{\pm} \end{pmatrix}. \tag{22}$$

Here, $\boldsymbol{\mathcal{Z}}_2 = \left(A_2^-, B_2^-, C_2^-, A_2^+, B_2^+, C_2^+\right)^{\mathrm{T}}$ are the wavenumber-dependent constants of domain-2 and $\boldsymbol{\mathcal{Z}}_{13} = (A_1, B_1, C_1, A_3, B_3, C_3)^{\mathrm{T}}$ are the wavenumber-dependent constants of domain-1 and 3.

Finally, by making use of the boundary conditions of velocity continuity stated by Eq. (8), the wavenumber-dependent functions associated with domain 2 (abbreviated by $\boldsymbol{\mathcal{Z}}_2$) can readily be expressed in terms of those associated with domains 1 and 3 (abbreviated by $\boldsymbol{\mathcal{Z}}_{13}$). Due to their complexity and lengthiness, the corresponding expressions have been omitted here.

Following the well-established recipes by Sneddon [64] and Copson [65], we introduce new unknown functions $\mathcal{G}_i : [0, R] \to \mathbb{R}$, for $i = 1, \ldots, 6$, and seek the solution of the integral equations stated by Eqs. (16) in the integral form

$$g_i(\lambda) = 2\lambda^{\frac{1}{2}} \int_0^R \mathcal{G}_i(t) J_{\frac{3}{2}}(\lambda t)\,\mathrm{d}t\,, \quad i \in \{1,4\}\,, \tag{23a}$$

$$g_i(\lambda) = 2\lambda^{\frac{1}{2}} \int_0^R \mathcal{G}_i(t) J_{\frac{1}{2}}(\lambda t)\,\mathrm{d}t\,, \quad i \in \{2,5\}\,, \tag{23b}$$

$$g_i(\lambda) = 2\lambda^{\frac{1}{2}} \int_0^R \mathcal{G}_i(t) J_{\frac{5}{2}}(\lambda t)\,\mathrm{d}t\,, \quad i \in \{3,6\}\,. \tag{23c}$$

The prime advantage of adopting this form of solution is that the outer region boundary conditions (16) are automatically satisfied upon making use of the following identity [63],

$$\int_0^\infty \lambda^{\frac{1}{2}} J_\nu(\lambda r) J_{\nu+\frac{1}{2}}(\lambda t)\,\mathrm{d}\lambda = 0 \qquad (0 < t < r)\,, \tag{24}$$

where ν is a positive integer.

Then, by changing the order of integration with respect to variables t and λ, the inner problem (12) reduces to a set of six integral equations of the form

$$\sum_{j=1}^{6} \int_0^R K_{ij}(r,t)\mathcal{G}_j(t)\,\mathrm{d}t = \Xi_i(r)\,, \quad i = 1, \ldots, 6\,, \tag{25}$$

wherein $\boldsymbol{\Xi} := \left(\xi_0^+, \xi_0^-, \xi_1^+, \xi_1^-, \xi_2^+, \xi_2^-\right)$ are the radially symmetric functions given by Eqs. (15). The kernel functions K_{ij}, with $i, j = 1, \ldots, 6$, entail improper (infinite) integrals with respect to the wavenumber λ (see Appendix for their expressions), which can be evaluated both numerically [66] and analytically. In the present work, we have adopted the latter route and obtained closed form expressions of these integrals. Equations (25) form a system of coupled Fredholm integral equations of the first kind for the final unknown functions $\mathcal{G}_i(t)$.

1. *Numerical solution of integral equations*

The complicated kernel functions appearing in Eqs. (25) prohibits us from obtaining analytical solutions for the functions $\mathcal{G}_i(t)$. Therefore, we must turn to numerical procedures. We employ the Legendre-Gauss quadrature [67] and evaluate the integrals at N Gaussian nodes in the interval $[0, R]$. This reduces the system of integral equations to a linear system of $6N$ equations, which can be easily solved using standard numerical methods [68]. With the known discrete values of $\mathcal{G}_i(t_j)$, where $i = 1, \ldots, 6$ and $j = 1, \ldots, N$, we again use a similar quadrature technique to evaluate the integrations in Eqs. (23) with respect to the variable t.

To tackle the improper integrals with respect to the variable λ in the interval $[0,\infty)$ in Eqs.(7a-c), we employ a variable transformation of the form $\lambda = \tan u$. This provides integrands in the changed integration limit, $u \in [0, \pi/2]$. Following this, we again use the Legendre-Gauss quadrature rule to evaluate discrete values of $g_i(u_m)$ at M Gaussian nodes, where $m \in [1, M]$.

Having obtained the variables $g_i(u_m)$, we proceed to recover the wavenumber-dependent quantities $\boldsymbol{\mathcal{Z}}_{13}$ and $\boldsymbol{\mathcal{Z}}_2$ using Eqs. (17) and obtain the velocity fields by performing integrations with respect to the wavenumber λ, as depicted in Eqs.(7a-c). Although the present methodology may seem complicated at a first sight, the method alleviates the need to solve a differential equation using a direct discretization technique in a three dimensional domain and provides an alternative formulation demanding only one-dimensional numerical quadrature. A detailed grid independence test related to the choice of quadrature points has been provided in Appendix **??**.

2. *Comparison with FEM simulations*

For validation, we compare the solutions with numerical finite element simulations. To discretize the Stokes equations, we use quadratic finite elements on an irregular hexahedral grid. As the quadratic equal order approach is not inf-sup stable, local projection stabilization is added [69]. The computational domain is artificially restricted to a hexahedron with side lengths $10R \times 10R \times 10H$. On the outer boundary the no-stress condition $[\eta(\boldsymbol{\nabla} v + \boldsymbol{\nabla} \boldsymbol{v}^T) - p\boldsymbol{I}] \cdot \boldsymbol{n} = 0$ is set. The flow is driven by the point force which is integrated exactly into the weak formulation as a Dirac on the right-hand side. Quadratic isoparametric finite elements [70, Sec. 4.2.3] are used to approximate the geometry of the two disks.

In order to resolve the singularity, the computational mesh is adaptively refined with highest resolution along the two disks and in particular at the position of the singularity. The finest discretization used to produce the results involve about 15 million degrees of freedom. The resulting linear systems of equations are inverted with a parallel multigrid solver [71]. All computations are performed in the finite element software library Gascoigne 3d [72].

D. Infinite plate limit, $R \to \infty$

In the limit of infinitely extended disks, the inner problem stated by Eqs. (12) becomes valid throughout the whole semi-infinite domain $r \in [0, \infty)$. Then, the unknown functions $g_i(\lambda)$ can be determined by transforming the auxiliary functions defined in Eqs. (15). This is achieved by applying the Hankel transform [73] of the form

$$\widehat{\xi}_\nu^{\pm}(\lambda) = \int_0^\infty r \xi_\nu^{\pm}(r) J_\nu(\lambda r) \mathrm{d}r \qquad \nu \in \{0,1,2\}. \tag{26}$$

A subsequent use of the orthogonality property of Bessel functions [63]

$$\int_0^\infty r J_\nu(\lambda r) J_\nu(\lambda' r)\, \mathrm{d}r = \lambda^{-1}\, \delta\,(\lambda - \lambda') \tag{27}$$

leaves us with a system of linear equations to be solved for $\boldsymbol{g} = (g_1, g_2, g_3, g_4, g_5, g_6)^{\mathrm{T}}$. Specifically,

$$\boldsymbol{\Lambda} \cdot \boldsymbol{g} = \widehat{\boldsymbol{\xi}}, \tag{28}$$

where

$$\boldsymbol{\Lambda} = \begin{pmatrix} 0 & 3\delta_1 & -\delta_1 & 2\delta_2 & \delta_4 & \delta_3 \\ 2\delta_2 & -\delta_4 & -\delta_3 & 0 & -3\delta_1 & \delta_1 \\ 2\delta_1 & 0 & 0 & -2\delta_3 & -\delta_2 & -\delta_2 \\ 2\delta_3 & -\delta_2 & -\delta_2 & -2\delta_1 & 0 & 0 \\ 0 & -\delta_1 & 3\delta_1 & 2\delta_2 & \delta_3 & \delta_4 \\ 2\delta_2 & -\delta_3 & -\delta_4 & 0 & \delta_1 & -3\delta_1 \end{pmatrix}, \tag{29}$$

where we have defined $\delta_1 = 1/\left(8\lambda^2\right)$, $\delta_2 = e^{-\lambda}/\left(8\lambda\right)$, $\delta_3 = (\lambda+1)\, e^{-\lambda}/\left(8\lambda^2\right)$, and $\delta_4 = (\lambda-3)\, e^{-\lambda}/\left(8\lambda^2\right)$. In addition, $\widehat{\boldsymbol{\xi}} = \left(\tau_1^+, \tau_1^-, \tau_2^+, \tau_2^-, \tau_3^+, \tau_3^-\right)^{\mathrm{T}}$ wherein $\tau_1^{\pm} = (3/\lambda \mp h - 1/2)\, e^{-\lambda(1/2 \pm h)}$, $\tau_2^{\pm} = \pm\,(1/2 \pm h)\, e^{-\lambda(1/2\pm h)}$, and $\tau_3^{\pm} = -\,(1/\lambda \pm h + 1/2)\, e^{-\lambda(1/2\pm h)}$.

The linear system stated by Eq. (28) can readily be solved analytically, giving compact expressions for the unknowns wavenumber-dependent functions $\boldsymbol{g}$. The expressions for $\boldsymbol{\mathcal{Z}}_2$ and $\boldsymbol{\mathcal{Z}}_{13}$ can subsequently be obtained by making use of Eq. (17).

III. RESULTS AND DISCUSSIONS

A. Hydrodynamic mobility

In the study of suspension mechanics [75, 76], the hydrodynamic mobility function serves as a means for relating the particle velocity with the force experienced by it. In case of a particle translating in an unbounded Newtonian fluid, the familiar Stokes law states the particle mobility as $\mu_0 = 1/(6\pi\eta a)$, where a is the particle radius. To investigate the influence of the disks on the drag force experienced by a point-like particle that is forced to move parallel to the disk surfaces and at the time of observation is just located on the center axis of the setup, we analyze the leading-order correction to the hydrodynamic mobility when compared to the bulk situation in the absence of the disks. This quantity can be obtained by evaluating the image flow field at the particle position. Specifically,

$$\Delta\mu = F^{-1} \lim_{(r,z)\to(0,h)} v_x^*\,. \tag{30}$$

Rescaling by the bulk mobility μ_0, we define the scaled leading-order correction factor to the Stokes mobility as

$$k = -\frac{1}{a}\frac{\Delta\mu}{\mu_0}. \tag{31}$$

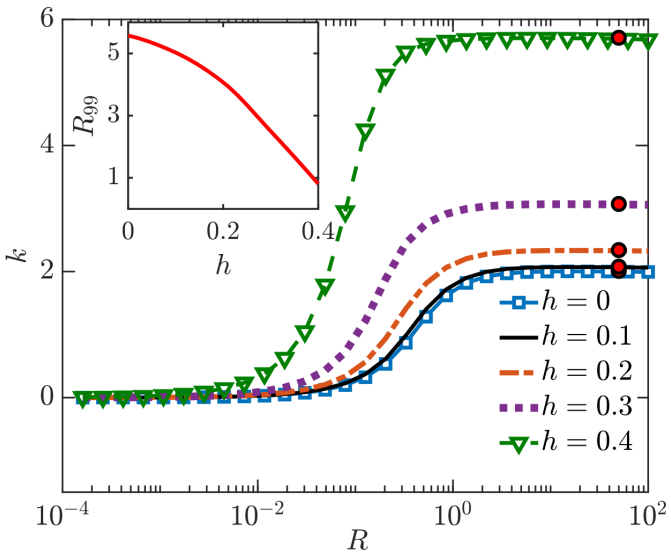

Figure 2. Mobility correction factor k vs. disk radius R for the forced point-like particle located at different vertical distances h from the center between the two coaxially arranged disks. The red markers represent the results of Swan and Brady [74]. Inset shows the variations of the radius R_{99}, a measure for the disk size from where the mobility becomes nearly identical to the one between infinitely extended disks, with the distance h.

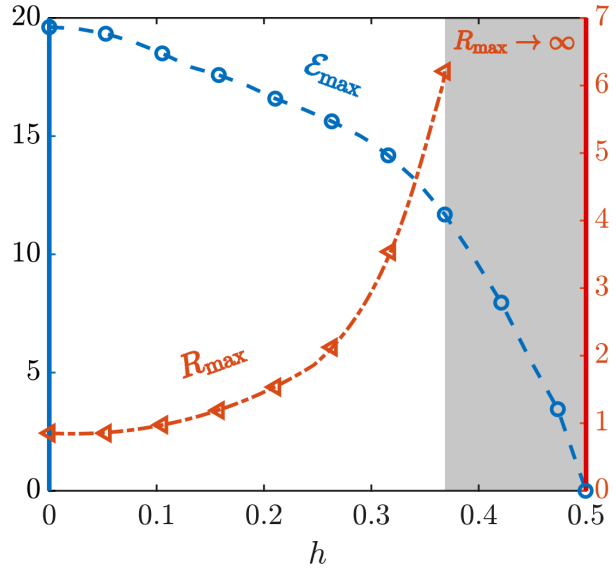

Figure 3. The left axis is associated with the maximum relative error in the mobility correction factor using the Oseen's superposition in comparison to our exact solution. Moreover, the right axis identifies the disk radius for which each value of $\mathcal{E}_{\max}$ was found. In the region marked in gray, $R_{\max}$ continues to diverge towards infinity.

Using the exact solution, the correction factor can be written in the integral form

$$k = \frac{3}{8}\int_0^\infty \lambda \Big(\left(\left(A_2^- \lambda - B_2^-\right) h - A_2^- - C_2^- \right) e^{-\lambda h} - e^{\lambda h} \left(\left(A_2^+ \lambda + B_2^+\right) h + A_2^+ + C_2^+ \right) \Big)\, \mathrm{d}\lambda. \tag{32}$$

Figure 2 depicts the variation of the leading order mobility correction factor versus the radius of the coaxially positioned disks for different vertical locations of the Stokeslet singularity. In the extreme limit where the disk radius is high enough to exhibit the characteristics of the infinitely extended flat plates, the factor k reaches an asymptotic value. The decreasing magnitude of the mobility correction factor k with decreasing radius of the disks indicates reduced resistance to particle motion. In the limit $R \to \infty$, the correction factor is found to be in full agreement with the solution reported by Swan and Brady [74] who employed a two-dimensional Fourier transform technique.

To quantify the cut-off radius below which the finite disk size becomes important, we calculate the disk radius, R_{99}, for which 99% of the mobility correction between infinitely extended disks is achieved. The inset to Fig. 2 shows that the radius R_{99} is maximum at $h = 0$ with a value of $R_{99} \simeq 5.58$. This value can readily be compared to its corresponding value of about 0.62 reported earlier for a Stokeslet acting normal to the disks [55]. This suggests an intrinsically distinct nature of the finite-disk effect on the movement of differently oriented point particles. In addition, the gradual decrease in R_{99} with the distance h signifies the fact that the disk finiteness becomes more and more crucial as the Stokeslet is located further away from of the surface of the closer disk.

1. *Comparison with Oseen's approximation*

In the following, we examine the accuracy and appropriateness of the linear superposition approximation suggested by Oseen [77]. In this approach, the hydrodynamic mobility between two parallel walls could appropriately be determined by superimposing the individual contributions arising from each wall independently. Accordingly, the mixed boundary conditions are no longer satisfied at the planes containing the two disks. To assess the success of this approximation for the finiteness of the confining disks, we make use of the single-disk solution reported earlier by Miyazaki [78]. Using our notation, the mobility correction factor near a single disk can be written in a closed form as [59]

$$\frac{\Delta\mu}{\mu_0} = -\frac{3}{4\pi}\left(\frac{3+5\xi^2}{(1+\xi^2)^2} + \frac{3}{\xi}\arctan\left(\frac{1}{\xi}\right)\right)\frac{a}{R}, \tag{33}$$

where $\xi = b/R$ with b denoting the distance between the particle and the center of the disk under consideration.

Following Oseen's approach, the leading-order correction factor to the hydrodynamic mobility can be approximated

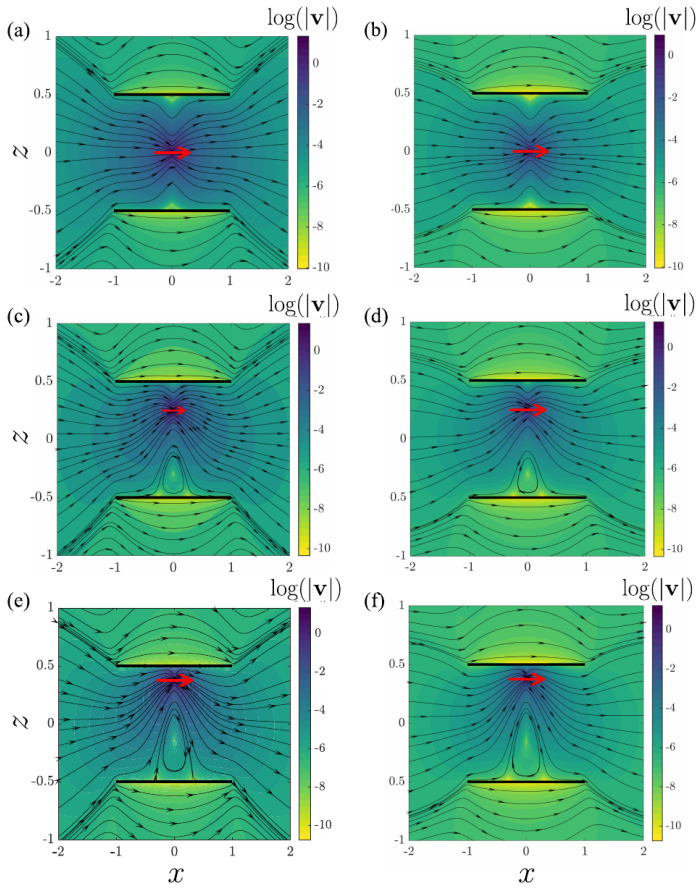

Figure 4. Flow field induced by a Stokeslet located at different vertical locations h. The top to bottom panels represent the cases with $h = 0, 0.25$ and 0.375, respectively. Left panels (a),(c), and (e) represent the results of the present semi-analytical theory, while the results of the corresponding numerical simulations are shown for comparison in the right panels (b), (d), and (f). In all the cases, $R = 1$ has been chosen.

by adding the leading-order corrections resulting from the individual disks. Then,

$$k_{\mathrm{Sup}} = -\frac{1}{a}\left(\left.\frac{\Delta\mu}{\mu_0}\right|_{b=\frac{1}{2}-h} + \left.\frac{\Delta\mu}{\mu_0}\right|_{b=\frac{1}{2}+h}\right). \qquad (34)$$

To probe the appropriateness of Oseen's approximation, we calculate the error $\mathcal{E}$ relative to the exact solution presented in section III A. In Fig. 3 we plot the maximum error $\mathcal{E}_{\max}$ obtained in the superposition approximation for a specific vertical distance h of the point-like particle from the center of the setup. We also portray the radius of the disks corresponding to that maximum error $R_{\max}$. The figure depicts that the approximate results are highly erroneous as the particle locates towards the mid-plane between the disks, implying up to about 20% error for $h = 0$. This maximum error is found to be reached for the radius of the disks $R \simeq 1$. The highest error is especially important considering the fact that the finite size of disks

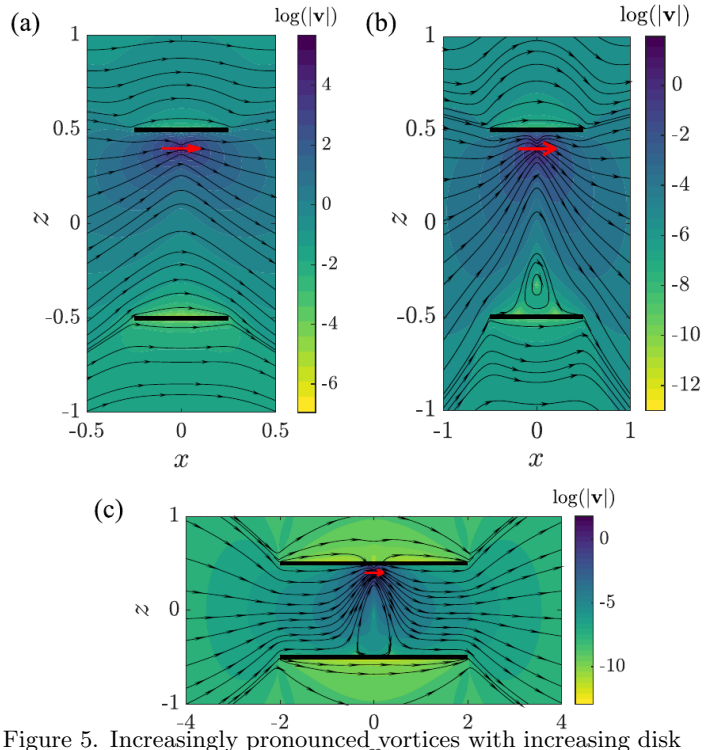

Figure 5. Increasingly pronounced vortices with increasing disk radius. Panels (a),(b), and (c) correspond to the cases of $R = 0.25, 0.5$ and 2, respectively. In all cases, $h = 0.4$.

has a significant impact on the mobility in this particular situation, as quantified in Fig. 2. It can also be inferred from Fig. 3 that, as the particle is located closer to one of the disks, the maximum error reduces monotonically and eventually vanishes altogether as $h \to 1/2$. The radius of the disks $R_{\max}$ corresponding to the maximum error increases monotonically with h and diverges to infinity for $h \to 1/2$.

Consequently, it can be concluded that the superposition approximation might generally work well except in the region close to the mid-plane between the two disks where the approximation fails to capture the correct trend of variation in the mobility correction factor.

B. Description of flow field

The flow disturbances created by the point force singularity pointing into a direction between the two disks strongly depend on the vertical location h of the singularity. In Fig. 4, the velocity streamlines and the velocity magnitude have been evaluated for three values of h while the radius of the disks is set to $R = 1$. The corresponding results from finite element simulations in the right panels show very good agreement with our semi-analytical theory. For $h = 0$, the velocity field is symmetric with respect to the mid-plane, as expected. We can also observe the existence of small vortices located near the disks. However, as the Stokeslet approaches one of the

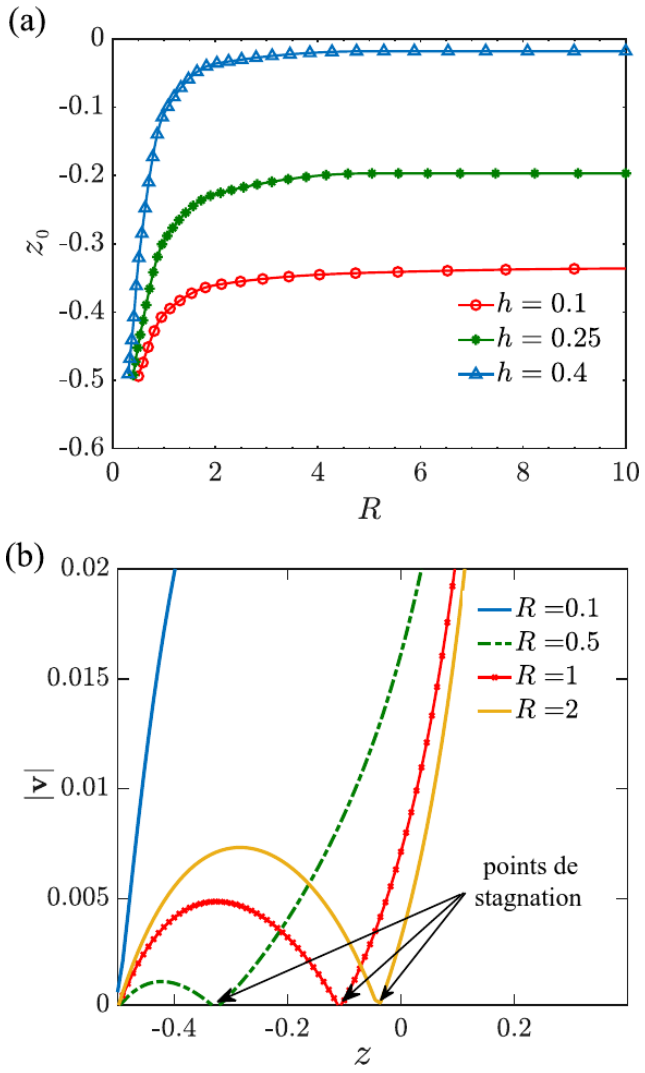

Figure 6. (a) Variation of the vertical position of the stagnation point z_0 with increasing disk radius R for different vertical locations h of the flow-inducing Stokeslet. (b) highlights location of the stagnation points as we vertically traverse from the bottom disk to the location $(x, z) = (0, 0.4)$ of the Stokeslet.

disks, this symmetric pattern is notably distorted. Due to flow continuity, a corresponding enhancement in the circulatory flow pattern is observed adjacent to the disk farther away from the Stokeslet.

While the varying location of the Stokeslet essentially gives an assessment of the wall-mediated flow hindrance, the varying disk radius indicates the relative contributions of the solid surfaces and no-obstacle zones in the $z = \pm 1/2$ planes. Thus, to delve deeper into the flow patterns, we have shown the velocity field for varying disk radius, but for a fixed location of the Stokeslet in Fig. 5. Apparently, the bigger vortex near the farther disk gets stronger with increasing disk radius, and a corresponding suppression of the other vortex occurs.

A systematic evaluation of the vortex existence and location is performed by analyzing the vertical location z_0 of the stagnation points that appear in the flow field at $x = 0$, here below the Stokeslet location for the demonstrations in these figures. According to Fig. 6(a), such a stagnation point will appear as the disk radius exceeds a low value. This lower limit has been found as $R = 0.4$ and 0.3 for $h = 0.1$ and 0.4, respectively. With further increase in disk radius, the no-slip contribution in the flow field on the surfaces of the disks begins to dominate the influence of the stress continuity zone in the disk planes at $z = \pm 1/2$ for $r > R$. The stagnation point moves further away from the nearby disk with increasing radius R of the disks, as portrayed in Fig. 6(b). Finally, in the limit of $R \to \infty$, the location of the analyzed stagnation points does not change any further and saturates to a constant value for that particular vertical location h of the Stokeslet.

IV. CONCLUSIONS

To summarize, we presented a semi-analytical theory that describes the flow field induced by a point-force singularity acting parallel to two coaxially positioned no-slip disks. We formulate the solution of the fluid mechanics equations as a standard mixed boundary value problem which we subsequently reduced into a system of dual integral equations. We showed that the solution methodology for the Green's functions require only one-dimensional numerical quadrature and thus alleviating the need to solve the hydrodynamic equations using direct discretization techniques in the whole three dimensional spatial domain. Thereupon, we provided an integral formulation of the leading-order correction to the hydrodynamic mobility function of a point-like particle and assessed the accuracy and appropriateness of the simplistic superposition approximation. We found that this approximation does well far away from the mid-plane but can lead to as high a 20% error otherwise.

In the present contribution, we assumed for simplicity that the point force is acting on the axis of the two coaxially positioned rigid disk. It would be of great interest to investigate the general situation of arbitrary position within the finite-sized channel. We argue that the dual integral equations formulation may prove challenging in this situation thus requiring a fundamentally different approach, e.g. using the Green and Neumann functions supplemented by the edge function technique. Additionally, it would be of interest to elaborate on the remaining components of the mobility tensor including the hydrodynamic coupling and rotational mobilities. These aspects would be of big interest to be examined in a future investigation.

ACKNOWLEDGMENTS

The author would like thank A. Poddar for early collaboration and technical support, for various stimulating discussions, and for assistance and help in the preparation of figures in the manuscript. In addition, he would like to thank S. Chakraborty and A. Bandopadhyay for a valuable discussion, T. Richter for providing the finite-element simulations data, A. M. Menzel and H. Löwen for insightful suggestions. The author gratefully acknowledge support from the DFG (Deutsche Forschungsgemeinschaft) through the project DA 2107/1–1.

[1] M. D. Graham, "Fluid dynamics of dissolved polymer molecules in confined geometries," Ann. Rev. Fluid Mech. **43**, 273–298 (2011).

[2] H. Diamant, "Hydrodynamic interaction in confined geometries," J. Phys. Soc. Japan **78**, 041002–041002 (2009).

[3] J. Nilsson, M. Evander, B. Hammarström, and T. Laurell, "Review of cell and particle trapping in microfluidic systems," Anal. Chim. Acta **649**, 141–157 (2009).

[4] M. Yamada, W. Seko, T. Yanai, K. Ninomiya, and M. Seki, "Slanted, asymmetric microfluidic lattices as size-selective sieves for continuous particle/cell sorting," Lab Chip **17**, 304–314 (2017).

[5] S. Zhang, Y. Wang, P. Onck, and J. den Toonder, "A concise review of microfluidic particle manipulation methods," Microfluid. Nanofluidics **24**, 1–20 (2020).

[6] G. Kunti, T. Agarwal, A. Bhattacharya, T. K. Maiti, and S. Chakraborty, "On-chip concentration and patterning of biological cells using interplay of electrical and thermal fields," Anal. Chem. **92**, 838–844 (2019).

[7] N. Zhang, H. Tan, and E. S. Yeung, "Automated and integrated system for high-throughput dna genotyping directly from blood," Anal. Chem. **71**, 1138–1145 (1999).

[8] C.-W. Kan, C. P. Fredlake, E. A. Doherty, and A. E. Barron, "DNA sequencing and genotyping in miniaturized electrophoresis systems," Electrophoresis **25**, 3564–3588 (2004).

[9] X. Wang, S. Wang, V. Veerappan, C. K. Byun, H. Nguyen, B. Gendhar, R. D. Allen, and S. Liu, "Bare nanocapillary for DNA separation and genotyping analysis in gel-free solutions without application of external electric field," Anal. Chem. **80**, 5583–5589 (2008).

[10] N. François, D. Lasne, Y. Amarouchene, B. Lounis, and H. Kellay, "Drag enhancement with polymers," Phys. Rev. Lett. **100**, 018302 (2008).

[11] N. François, Y. Amarouchene, B. Lounis, and H. Kellay, "Polymer conformations and hysteretic stresses in nonstationary flows of polymer solutions," Europhys. Lett. **86**, 34002 (2009).

[12] I. Dufour, A. Maali, Y. Amarouchene, C. Ayela, B. Caillard, A. Darwiche, M. Guirardel, H. Kellay, E. Lemaire, F. Mathieu, *et al.*, "The microcantilever: A versatile tool for measuring the rheological properties of complex fluids," J. Sens. **2012** (2012).

[13] A. Darwiche, F. Ingremeau, Y. Amarouchene, A. Maali, I. Dufour, and H. Kellay, "Rheology of polymer solutions using colloidal-probe atomic force microscopy," Phys. Rev. E **87**, 062601 (2013).

[14] S. Kim and S. J. Karrila, *Microhydrodynamics: Principles and Selected Applications* (Courier Corporation, New York, U.S.A., 2013).

[15] J. Happel and H. Brenner, *Low Reynolds number hydrodynamics, 1965* (1983).

[16] R. Hsu and P. Ganatos, "The motion of a rigid body in viscous fluid bounded by a plane wall," J. Fluid Mech. **207**, 29–72 (1989).

[17] I. Pagonabarraga, M. H. J. Hagen, C. P. Lowe, and D. Frenkel, "Algebraic decay of velocity fluctuations near a wall," Phys. Rev. E **58**, 7288–7295 (1998).

[18] M. A. Bevan and D. C. Prieve, "Hindered diffusion of colloidal particles very near to a wall: Revisited," J. Chem. Phys. **113**, 1228–1236 (2000).

[19] J. T. Padding and W. J. Briels, "Translational and rotational friction on a colloidal rod near a wall," J. Chem. Phys. **132**, 054511 (2010).

[20] P. Holmqvist, J. K. G. Dhont, and P. R. Lang, "Colloidal dynamics near a wall studied by evanescent wave light scattering: Experimental and theoretical improvements and methodological limitations," J. Chem. Phys. **126**, 044707 (2007).

[21] T. Franosch, M. Grimm, M. Belushkin, F. M. Mor, G. Foffi, L. Forró, and S. Jeney, "Resonances arising from hydrodynamic memory in Brownian motion," Nature **478**, 85–88 (2011).

[22] S. A. Rogers, M. Lisicki, B. Cichocki, J. K. G. Dhont, and P. R. Lang, "Rotational diffusion of spherical colloids close to a wall," Phys. Rev. Lett. **109**, 098305 (2012).

[23] M. Lisicki, B. Cichocki, J. K. G. Dhont, and P. R. Lang, "One-particle correlation function in evanescent wave dynamic light scattering," J. Chem. Phys. **136**, 204704 (2012).

[24] M. Lisicki, B. Cichocki, S. A. Rogers, J. K. G. Dhont, and P. R. Lang, "Translational and rotational near-wall diffusion of spherical colloids studied by evanescent wave scattering," Soft Matter **10**, 4312–4323 (2014).

[25] A. Poddar, A. Bandopadhyay, and S. Chakraborty, "Steering a thermally activated micromotor with a nearby isothermal wall," J. Fluid Mech. **915**, A22 (2021).

[26] E. Lauga and T. M. Squires, "Brownian motion near a partial-slip boundary: A local probe of the no-slip condition," Phys. Fluids **17**, 103102 (2005).

[27] B. U. Felderhof, "Hydrodynamic force on a particle oscillating in a viscous fluid near a wall with dynamic partial-slip boundary condition," Phys. Rev. E **85**, 046303 (2012).

[28] A. Poddar, A. Bandopadhyay, and S. Chakraborty, J. Fluid Mech. , A11 (2020).

[29] J. Bławzdziewicz, V. Cristini, and M. Loewenberg, "Stokes flow in the presence of a planar interface covered with incompressible surfactant," Phys. Fluids **11**, 251–258 (1999).

[30] J. Blawzdziewicz, E. Wajnryb, and M. Loewenberg, "Hydrodynamic interactions and collision efficiencies of spherical drops covered with an incompressible surfactant film," J. Fluid Mech. **395**, 29–59 (1999).

[31] V. A. Shaik and A. M. Ardekani, "Point force singularities outside a drop covered with an incompressible surfactant: Image systems and their applications," Phys. Rev. Fluids **2**, 113606 (2017).

[32] C. Kurzthaler, L. Zhu, A. A. Pahlavan, and H. A. Stone, "Particle motion nearby rough surfaces," Phys. Rev. Fluids **5**, 082101 (2020).

[33] T. Bickel, "Brownian motion near a liquid-like membrane," Eur. Phys. J. E **20**, 379–385 (2006).

[34] T. Bickel, "Hindered mobility of a particle near a soft interface," Phys. Rev. E **75**, 041403 (2007).

[35] T. Salez and L. Mahadevan, "Elastohydrodynamics of a sliding, spinning and sedimenting cylinder near a soft wall," J. Fluid Mech. **779**, 181–196 (2015).

[36] A. Daddi-Moussa-Ider, A. Guckenberger, and S. Gekle, "Long-lived anomalous thermal diffusion induced by elastic cell membranes on nearby particles," Phys. Rev. E **93**, 012612 (2016).

[37] A. Daddi-Moussa-Ider and S. Gekle, "Brownian motion near an elastic cell membrane: A theoretical study," Eur. Phys. J. E **41**, 1–13 (2018).

[38] A. Daddi-Moussa-Ider, M. Lisicki, S. Gekle, A. M. Menzel, and H. Löwen, "Hydrodynamic coupling and rotational mobilities nearby planar elastic membranes," J. Chem. Phys. **149**, 014901 (2018).

[39] B. Rallabandi, B. Saintyves, T. Jules, T. Salez, C. Schönecker, L. Mahadevan, and H. A. Stone, "Rotation of an immersed cylinder sliding near a thin elastic coating," Phys. Rev. Fluids **2**, 074102 (2017).

[40] B. Rallabandi, N. Oppenheimer, M. Y. B. Zion, and H. A. Stone, "Membrane-induced hydroelastic migration of a particle surfing its own wave," Nat. Phys. , 1 (2018).

[41] B. Saintyves, T. Jules, T. Salez, and L. Mahadevan, "Self-sustained lift and low friction via soft lubrication," Proc. Nat. Acad. Sci. **113**, 5847–5849 (2016).

[42] G. Fulford and J. Blake, "On the motion of a slender body near an interface between two immiscible liquids at very low reynolds numbers," J. Fluid Mech. **127**, 203–217 (1983).

[43] W. Wang and P. Huang, "Anisotropic mobility of particles near the interface of two immiscible liquids," Phys. Fluids **26**, 092003 (2014).

[44] H. Faxén, *Einwirkung der Gefässwände auf den Widerstand gegen die Bewegung einer kleinen Kugel in einer zähen Flüssigkeit*, Ph.D. thesis, Uppsala University, Uppsala, Sweden (1921).

[45] N. Liron and S. Mochon, "Stokes flow for a stokeslet between two parallel flat plates," J. Eng. Math. **10**, 287–303 (1976).

[46] S. Bhattacharya and J. Bławzdziewicz, "Image system for Stokes-flow singularity between two parallel planar walls," J. Math. Phys. **43**, 5720–5731 (2002).

[47] J. W. Swan and J. F. Brady, "Particle motion between parallel walls: Hydrodynamics and simulation," Phys. Fluids **22**, 103301 (2010).

[48] P. Ganatos, R. Pfeffer, and S. Weinbaum, "A strong interaction theory for the creeping motion of a sphere between plane parallel boundaries. part 2. parallel motion," J. Fluid Mech. **99**, 755–783 (1980).

[49] P. Ganatos, S. Weinbaum, and R. Pfeffer, "A strong interaction theory for the creeping motion of a sphere between plane parallel boundaries. part 1. perpendicular motion," J. Fluid Mech. **99**, 739–753 (1980).

[50] E. R. Dufresne, D. Altman, and D. G. Grier, "Brownian dynamics of a sphere between parallel walls," Europhys. Lett. **53**, 264 (2001).

[51] L. Lobry and N. Ostrowsky, "Diffusion of Brownian particles trapped between two walls: Theory and dynamic-light-scattering measurements," Phys. Rev. B **53**, 12050–12056 (1996).

[52] L. P. Faucheux and A. J. Libchaber, "Confined Brownian motion," Phys. Rev. E **49**, 5158–5163 (1994).

[53] B. Lin, J. Yu, and S. A. Rice, "Direct measurements of constrained Brownian motion of an isolated sphere between two walls," Phys. Rev. E **62**, 3909–3919 (2000).

[54] B. Tränkle, D. Ruh, and A. Rohrbach, "Interaction dynamics of two diffusing particles: contact times and influence of nearby surfaces," Soft Matter **12**, 2729–2736 (2016).

[55] A. Daddi-Moussa-Ider, A. R. Sprenger, Y. Amarouchene, T. Salez, C. Schönecker, T. Richter, H. Löwen, and A. M. Menzel, "Axisymmetric Stokes flow due to a point-force singularity acting between two coaxially positioned rigid no-slip disks," J. Fluid Mech. **904** (2020).

[56] M.-U. Kim, "Axisymmetric Stokes flow due to a point force near a circular disk," J. Phys. Soc. Jpn. **52**, 449–455 (1983).

[57] A. Daddi-Moussa-Ider, M. Lisicki, H. Löwen, and A. M. Menzel, "Dynamics of a microswimmer–microplatelet composite," Phys. Fluids **32**, 021902 (2020).

[58] A. Daddi-Moussa-Ider, B. Kaoui, and H. Löwen, "Axisymmetric flow due to a Stokeslet near a finite-sized elastic membrane," J. Phys. Soc. Jpn. **88**, 054401 (2019).

[59] A. Daddi-Moussa-Ider, "Asymmetric Stokes flow induced by a transverse point force acting near a finite-sized elastic membrane," J. Phys. Soc. Jpn. **89**, 124401 (2020).

[60] M.-U. Kim and W.-K. Chung, "Axisymmetric slow viscous flow due to the motion of two equal coaxial disks," J. Phys. Soc. Jpn. **54**, 2874–2882 (1985).

[61] J. R. Blake, "A note on the image system for a Stokeslet in a no-slip boundary," Math. Proc. Cambridge Philos. Soc. **70**, 303 (1971).

[62] R. Shail and B. A. Packham, "Some asymmetric Stokes-flow problems," J. Eng. Math. **21**, 331 (1987).

[63] M. Abramowitz and I. A. Stegun, "Handbook of mathematical functions with formulas, graphs, and mathematical table," in *US Department of Commerce* (National Bureau of Standards Applied Mathematics series 55, 1965).

[64] I. N. Sneddon, "The elementary solution of dual integral equations," Glasgow Math. J. **4**, 108 (1960).

[65] E. T. Copson, "On certain dual integral equations," Glasgow Math. J. **5**, 21 (1961).

[66] J. P. Tanzosh and H. A. Stone, "A general approach for analyzing the arbitrary motion of a circular disk in a Stokes flow," Chem. Eng. Commun. **148**, 333–346 (1996).

[67] G. H. Golub and J. H. Welsch, "Calculation of Gauss quadrature rules," Math. Comput. **23**, 221–230 (1969).

[68] A. M. Ostrowski, *Solution of Equations and Systems of Equations: Pure and Applied Mathematics: A Series of Monographs and Textbooks, Vol. 9*, Vol. 9 (Elsevier, 2016).

[69] R. Becker and M. Braack, "A finite element pressure gradient stabilization for the Stokes equations based on

local projections," Calcolo **38**, 173–199 (2001).
[70] T. Richter, *Fluid-structure Interactions. Models, Analysis and Finite Elements*, Lecture notes in computational science and engineering, Vol. 118 (Springer, 2017).
[71] L. Failer and T. Richter, "A parallel Newton multigrid framework for monolithic fluid-structure interactions," J. Sci. Comput. **82** (2020).
[72] R. Becker, M. Braack, D. Meidner, T. Richter, and B. Vexler, "The finite element toolkit Gascoigne3d," (2020).
[73] R. Piessens, *The Hankel Transform*, Vol. 2 (CRC Press Second, Boca Raton, Florida, U.S.A., 2000).
[74] J. W. Swan and J. F. Brady, "Particle motion between parallel walls: Hydrodynamics and simulation," Phys. Fluids **22**, 103301 (2010).
[75] G. K. Batchelor, *An Introduction to Fluid Dynamics* (Cambridge University Press, Cambridge, U.K., 2000).
[76] E. Guazzelli and J. F. Morris, *A Physical Introduction to Suspension Dynamics*, Vol. 45 (Cambridge University Press, Cambridge, U.K., 2011).
[77] C. W. Oseen, "Neuere Methoden und Ergebnisse in der Hydrodynamik," (1928).
[78] T. Miyazaki, "The effect of a circular disk on the motion of a small particle in a viscous fluid," J. Phys. Soc. Jpn. **53**, 1017–1025 (1984).
[79] S. Wolfram, *Mathematica: A System for Doing Mathematics by Computer* (Addison Wesley Longman Publishing Co., Inc., Boston, MA, U.S.A., 1991).
[80] D. V. Widder, *Laplace Transform (PMS-6)* (Princeton University Press, New Jersey, U.S.A., 2015).